Confirmation of the random tiling hypothesis by polar calculus

Moritz Holzwarth, Johannes Roth, and Hans-Rainer Trebin*
Institute for Functional Matter and Quantum Technologies, University of Stuttgart, 70550 Stuttgart, Germany

(Received 5 March 2024; revised 3 May 2024; accepted 11 June 2024; published 1 July 2024)

The random tiling hypothesis, first proposed by Elser and Henley in the 1980s, states that quasicrystals are entropy-stabilized and, hence, are high-temperature phases. We confirm the hypothesis for a two-dimensional Tübingen triangle tiling, which arises in molecular dynamics simulations with a Lennard-Jones-Gauß potential, by investigating the temperature dependence of its two phason elastic constants λ_6 and λ_8. These are the second derivatives of the free energy $F(\chi_6, \chi_8, T)$ with respect to symmetrized phason strain modes χ_6 and χ_8. At $T = 0$, F has a saddle point by descending along the χ_8 direction. Therefore $\lambda_8 < 0$ characterizes the quasicrystal's initial instability. The configurational entropy due to phason flips turns F upwards at higher temperatures, reverses the sign of λ_8, and leads to a stable quasicrystal. We obtain this result by applying geometric methods in the form of the polar calculus, where the projection window $\mathcal{W}$ is divided into atomic domains $\mathcal{C}_i$ for each vertex environment. We extend the calculus to a dynamic one by separating the window into areas $\mathcal{P}_k$ that characterize the different kinds of phason flips. By phasonic deformation of the window, we can determine the types of flips and their frequency of occurrence in dependence on phason strain, perform energy relaxations by flips, and compute the configurational free energy. Previously, flips therein had been dealt with as uncorrelated and described as Ising spins. We consider nearest neighbor correlations between flips by extending the Ising to a Potts model and find that they constitute an important mechanism supporting the quasicrystal stability.

DOI: 10.1103/PhysRevB.110.024102

I. INTRODUCTION

Quasicrystals are condensed matter systems, whose diffraction patterns display noncrystallographic symmetries, for example, five, eight, or tenfold ones [1]. This is why they cannot be periodic structures, rather are modeled as aperiodic tessellations of space with more than one tile, as the famous Penrose tiling. Quasicrystals are aperiodic, because the number n of their reciprocal basis vectors which are linearly independent over the integers, exceeds their spatial dimension d. Hence, as a mathematical trick, one frequently describes them as projections from a higher- (n-) dimensional periodic lattice to a d-dimensional "physical" plane positioned therein under irrational angles [2]. Displacements of the vertices of the periodic lattice parallel to the plane give rise to the standard elastic degree of freedom, expressed by the strain tensor ϵ. But displacements orthogonal to the physical plane represent an additional "phason" degree of freedom, characterized by a phason strain tensor χ and generalized elastic constants (phonon, phason, and coupling) [3]. In the tiling picture phason strain shows up as flips of the tiling vertices. If fluctuations of the phason strain are present in equilibrium, then a quasicrystal becomes stabilized entropically. Elser [4] and Henley [5,6] proposed this scenario as random tiling hypothesis shortly after the discovery of quasicrystals by Dan Shechtman [7,8]. As a consequence, quasicrystals were high-temperature phases transforming at low temperatures into periodic crystals.

A numerical test of the random tiling hypothesis was performed in 2012 by Kiselev *et al.* [9] on the two-dimensional decagonal Tübingen triangle tiling (TTT) [10]. It was made possible by an interaction potential with two minima, the Lennard-Jones-Gauss (LJG) potential, which at a special choice of positions and depths of the minima stabilized a random version of the tiling in molecular dynamics (MD) simulations [11,12]. Phason strain χ was applied, characterized essentially by two symmetrized strain modes χ_6 and χ_8. The temperature dependent free energy $F(\chi_6, \chi_8, T)$ was measured. For the contribution of the phason flips to F, denoted configurational free energy F_{conf}, a model of independent Ising spins was applied, neglecting flip correlations. As second derivatives of F with respect to χ_6 and χ_8, the two phason elastic constants λ_6 and λ_8 were calculated. It turned out that with lowered temperature λ_8 vanished, rendering the quasicrystal unstable. Such a mechanism had been observed already by Bancel *et al.* in x-ray investigations of icosahedral Al-Cu-Fe [13,14]. There decreasing diffraction peak intensities and a transition to a periodic phase were explained by softening of a phason elastic constant.

Alternatively, energetic stabilization has been proposed for quasicrystals where the interactions enforce the matching rules for completely ordered systems [3]. It has been demonstrated that the required potentials had to show well-defined oscillations at more than five next-neighbor distances rendering this mechanism improbable [15]. Quasicrystalline structures in dendritic liquid crystals are enforced by frustrated tetrahedral close-packed structures of spherical micelles, i.e., by steric reasons [16] similar as in polymeric quasicrystals of *ABC* star polymers [17].

In the present paper, we confirm, using a purely geometric method characteristic for quasicrystals and denoted polar calculus [18], that a certain monatomic system with specified pairwise potential interactions exhibits a quasicrystal phase

*Contact author: trebin@itap.uni-stuttgart.de

that is entropically stabilized. Out of the numerical data of Kiselev *et al.* [9], we make use only of the single atom energies at $T = 0$ and the insight, that the only part of the phonon free energy contributing to the phason elastic constants is the ground state energy $E_0(\chi)$. In the polar calculus, the projection window $\mathcal{W}$ is divided into domains $\mathcal{C}_i$ for each vertex environment, allowing to calculate its relative portion. We go further and separate the window into sections $\mathcal{P}_k$ for the different kinds of flips, extending the polar calculus to a dynamic one. Constant phason strain deforms the window and its substructure, changing the proportions of vertex environments and flip types. For each value χ of phason strain, we perform energy relaxations by flips, compute the free energy of the relaxed state at $T = 0$ and its change with temperature due to the configurational free energy F_{conf}, and arrive at the temperature dependence of the phason elastic constants. Finally, the polar calculus also allows us to introduce next nearest neighbor correlations between flips by replacing the Ising with a Potts model [19].

In a most recent paper [20], it was demonstrated for a dodecagonal quasicrystal of a hard sphere mixture that it is stabilized by configurational entropy. The method and system are barely comparable to ours. We use realistic interactions and only one sort of atoms, thus are not troubled by the entropy of mixing.

In Sec. II, we inform how the TTT is constructed and how it is represented by two kinds of triangles, and—as primarily applied here—five types of polygons. The LJG potential is presented and the random tiling to which it gives rise in MD simulations. Furthermore, we list the nine vertex environments within an effective interaction radius $r_{\text{int}} = 2$ of the potential, which is twice the nearest neighbor distance. Section III refers to the free energy calculations by Kiselev *et al.* [9] for the phonon and the configurational part. In Sec. IV, we introduce the dynamic polar calculus by dividing the window $\mathcal{W}$ into areas $\mathcal{P}_k$ for the different flip types. The previous representation of the vertex flips by an Ising model is replaced by a Potts model with ten instead of two states. It takes into account correlations of neighboring flips and is denoted pentagon model. In Sec. V, the stability range of the random TTT is explored by following the temperature dependence of the phason elastic constants. It is confirmed that one of the constants, λ_8, starts from $T = 0$ with negative values. Due to configurational entropy, it turns positive at finite temperatures, in accordance with the random tiling hypothesis.

II. THE MODEL QUASICRYSTAL

A. LJG potential and Tübingen triangle tiling

In 2007 Engel and Trebin proposed a parametrized radially symmetric pair potential with two minima, denoted Lennard-Jones-Gauß (LJG) potential [11]:

$$V_{\text{LJG}}(r) = \frac{1}{r^{12}} - \frac{2}{r^6} - \epsilon \exp\left[-\frac{(r - r_0)^2}{2\sigma^2}\right], \qquad (1)$$

by which in certain parameter and temperature ranges they could grow two-dimensional monoatomic quasicrystals in MD simulations. For the parameters $r_0 = 1.53$, $\epsilon = 1.8$, and $\sigma^2 = 0.02$, they obtained a random form of the Tübingen triangle tiling (Fig. 1, right). Its two minima with a distance ratio of 1.512 close to the golden mean favor an easy realization of flips.

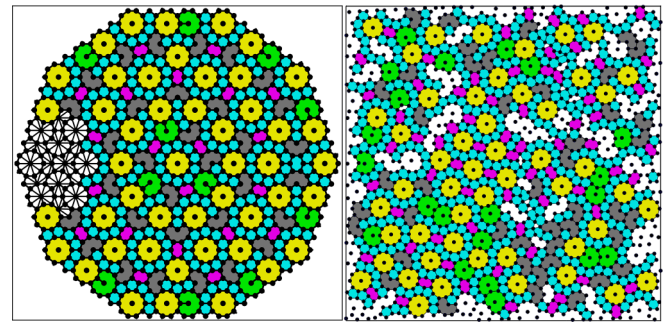

FIG. 1. (Left) Ordered TTT. Some of the original golden triangles are highlighted. (Right) Random TTT as a result of an MD simulation with the LJG potential.

The decagonal TTT was proposed in 1990 by Baake *et al.* [10]. It is related to the Penrose pattern and, in its basic form, is composed of thin and thick golden triangles. An alternative representation by polygons (regular and nonconvex decagons, nonagons, hexagons, and pentagons) is obtained by connecting nearest neighbors as in Figs. 1 and 2, left. The tiling can be constructed via a substitution rule or by projection from a four-dimensional hyperspace $\mathcal{H}$. Using the latter method, the TTT's vertices are projections of lattice points of a four-dimensional root lattice $\mathbb{A}_4$ onto a two-dimensional subspace of $\mathcal{H}$. Though four-dimensional, the hyperlattice is most naturally represented by the five vectors $\boldsymbol{a}_i$, $i \in \{0, 1, 2, 3, 4\}$ with

$$\boldsymbol{a}_i = \boldsymbol{e}_i - \boldsymbol{e}_{(i+1) \bmod 5}. \qquad (2)$$

The vectors $\boldsymbol{e}_i$ constitute the canonical basis of $\mathbb{R}^5$. The tenfold symmetry of $\mathbb{A}_4$ becomes apparent as the group D_{10} has a five-dimensional representation that simply permutes the basis vectors $\boldsymbol{a}_i$. There are two two-dimensional invariant subspaces of $\mathcal{H}$ with respect to D_{10}. The one in which the tiling is constructed is transforming according to the irreducible representation Γ_5 of D_{10} and is called parallel space $E^{\parallel}$. The other one, which is used to select the projected hyperlattice

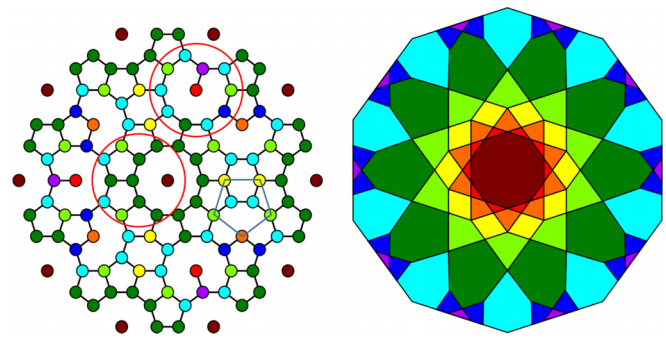

FIG. 2. (Left) A small patch of the decagonal TTT. The colors correspond to the distinct vertices as in Table I. Two vertices are marked with the interaction circle. The pentagon indicates one of the PC clusters dealt with in Sec. IV C. (Right) The window $\mathcal{W}$ in perp space is a regular decagon and is divided into atomic domains $\mathcal{C}_i$ for the corresponding vertices.

TABLE I. Vertices, their potential energies, and densities, from Ref. [9].

	Vertex	E_i	n_i/N
●	V_1	−19.6	τ^{-6}
●	V_2	−18.4	τ^{-9}
●	V_3	−17.2	$2\tau^{-8}$
●	V_4	−16.1	$2\tau^{-7}$
●	V_5	−14.5	$2\tau^{-6}$
●	V_6	−12.9	$4\tau^{-5}$
●	V_7	−11.3	$2\sqrt{5}\tau^{-6}$
●	V_8	−10.9	$4\tau^{-8}$
●	V_9	−9.0	τ^{-9}

points, is called perpendicular space $E^\perp$ and transforms according to Γ_7 [21]. Only $E^\parallel$ components of those hyperlattice points are considered as vertices in the TTT for which the $E^\perp$ component lies within a certain region called the projection window $\mathcal{W} \subset E^\perp$. In the case of the TTT, $\mathcal{W}$ is the projection of the Voronoi cell of $\mathbb{A}_4$ onto $E^\perp$. It has the shape of a regular decagon, see Fig. 2, right. The window is covered densely. The mapping between a projected point $v_j^\parallel$ in $E^\parallel$ and the projection $v_j^\perp$ in $\mathcal{W}$ is bijective.

Symmetry adapted orthonormal bases $\{\boldsymbol{b}_x^\parallel, \boldsymbol{b}_y^\parallel\}$ for $E^\parallel$ and $\{\boldsymbol{b}_x^\perp, \boldsymbol{b}_y^\perp\}$ for $E^\perp$, which together with corresponding two-dimensional canonical bases $\{e_x^\parallel, e_y^\parallel\}$, $\{e_x^\perp, e_y^\perp\}$ define the projection operators $\mathbf{P}^\parallel$ and $\mathbf{P}^\perp$ to both spaces, the vertices $\boldsymbol{d_i} \in \mathcal{H}$ of the Voronoi cell and the corners $d_i^\perp \in E^\perp$, $d_i^\parallel \in E^\parallel$ of the decagonal window are given in the Appendix.

Local shifts of $\mathcal{W}$ along $E^\perp$, represented by a displacement field $w_i(x_j^\parallel)$ and a phason strain tensor $\chi_{ij} = \partial_j w_i$ cause rearrangements of the tiling vertices by flips. A random tiling emerges from an isotropic distribution of thermally excited flips.

Our central observable for judging the stability of our random TTT is its free energy in dependence of temperature and applied average strain tensor χ. In continuum harmonic approximation the free phason elastic energy density per particle is [22]

$$F(\chi, T) = \tfrac{1}{2}\lambda_6(T)\left[\left(\chi_6^{(1)}\right)^2 + \left(\chi_6^{(2)}\right)^2\right] + \tfrac{1}{2}\lambda_8(T)\left[\left(\chi_8^{(1)}\right)^2 + \left(\chi_8^{(2)}\right)^2\right], \quad (3)$$

with symmetrized strain modes

$$\begin{bmatrix} \chi_6^{(1)} \\ \chi_6^{(2)} \\ \chi_8^{(1)} \\ \chi_8^{(2)} \end{bmatrix} = \frac{1}{\sqrt{2}} \begin{bmatrix} 1 & -1 & 0 & 0 \\ 0 & 0 & 1 & 1 \\ 1 & 1 & 0 & 0 \\ 0 & 0 & 1 & -1 \end{bmatrix} \begin{bmatrix} \chi_{11} \\ \chi_{22} \\ \chi_{12} \\ \chi_{21} \end{bmatrix}. \quad (4)$$

The phason elastic constants λ_6 and λ_8 are temperature dependent and are weighting strain contributions transforming according to the Γ_6 and Γ_8 irreducible representations of the symmetry group D_{10} [21]. In the following, we are applying only strain with $\chi_{12} = \chi_{21} = 0$. Therefore only $\chi_6^{(1)}$ and $\chi_8^{(1)}$ are nonzero and henceforth denoted χ_6 and χ_8. By varying them we determine λ_6 and λ_8.

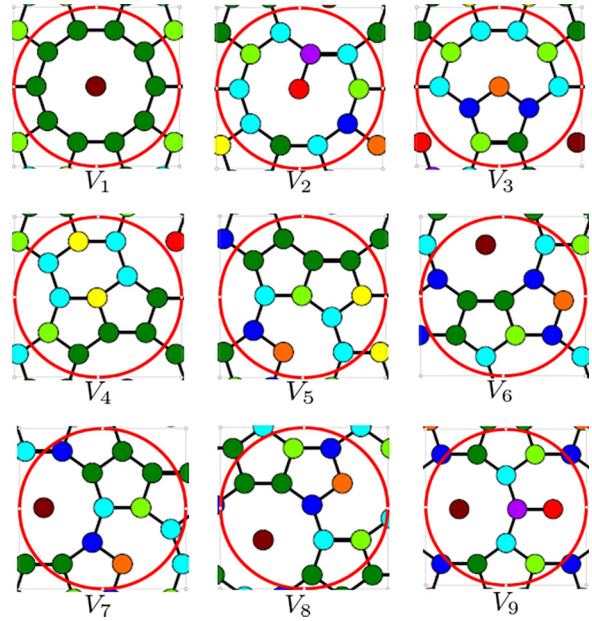

FIG. 3. The nine vertex environments of the TTT within a radius $r_{\text{int}} = 2$, enumerated in Table I and coded by the color of the central vertex.

B. Molecular dynamics calculations

The screenshot on the right of Fig. 1 results from MD simulations of 1600 particles with the LJG potential in an *NPT* ensemble at $T = 0.45$. The solid phase is melting in a first-order phase transition at $T = 0.56 \pm 0.02$. Monte Carlo (MC) simulations with the same potential had shown a transition to a Xi approximant at $T = 0.37 \pm 0.03$. Thus, from simulations, we can expect a stability range of the random TTT between $T = 0.37$ and 0.56.

C. Polar calculus and vertex environments

In the simulations, a cutoff radius of $r_c = 2.5$ was applied, however, it is justified to assume an interaction radius for each atom of $r_{\text{int}} = 2$, as for this value the potential energy is 2% of its maximal depth. For this interaction radius, there are up to rotations and reflections nine vertex environments V_i, given in Table I (from Ref. [9]) and pictured in Fig. 3. For two of them, the interaction circle is drawn in Fig. 2, left.

This is a confusing large vertex variety, compared to the one in periodic crystals. However, in quasicrystals there is an efficient bookkeeping tool for the vertices, denoted polar calculus [18].

The window $\mathcal{W}$ is subdivided into domains $\mathcal{C}_i$ of area $|\mathcal{C}_i|$, see Fig. 2, right. Vertices that are mapped into the same domain have the same neighborhood. The neighborhoods here are the vertex environments, with the same colors in direct as in orthogonal space. If in an area with N vertices, one counts n_i vertices of type i, the corresponding vertex density

$\rho_i \equiv n_i/N$ in the limit $N \to \infty$ is given by $\rho_i = |\mathcal{C}_i|/|\mathcal{W}|$ and is listed in column 4 of Table I.

Vertex V_i has potential energy

$$E_i = \sum_j V_{\mathrm{LJG}}(r_j), \qquad i = 1, \ldots 9. \tag{5}$$

The sum runs over the atoms j inside the disk of radius r_{int} with energy optimized separations r_j from the central atom at $T = 0$. For the perfect TTT, the configurational potential energy per atom at $T = 0$ follows as

$$E = \frac{1}{2}\sum_{i=1}^{9} \rho_i E_i, \tag{6}$$

where the factor $\frac{1}{2}$ avoids double counting of atoms.

Let us shortly repeat the principles of polar calculus. Take any atom configuration $\{v_j^{\parallel}\}$ in the tiling, where the positions are found via the projection operator $\mathbf{P}^{\parallel}$ and are expressed in the basis $\{e_k^{\parallel}\}$:

$$v_j^{\parallel} = \sum_k v_{jk} e_k^{\parallel}. \tag{7}$$

The corresponding position $v_j^{\perp}$ in $E^{\perp}$ is found simply by replacing $e_k^{\parallel}$ by $e_k^{\perp}$. Then, the window $\mathcal{W}$ is attached to each $E^{\perp}$ position. $\mathcal{W}$ is parameterized by its corners $d_l^{\perp}$, $l = 1, \ldots, 10$ (see Table II in Appendix). The domain $\mathcal{C}_i$ of the atom configuration is then the intersection of all these windows

$$\mathcal{C}_i = \bigcap_j (v_j^{\perp} + \mathcal{W}). \tag{8}$$

It can be calculated through triangulation, for which we have used the geometry package SHAPELY for PYTHON [23].

An alternative interpretation of the domain $\mathcal{C}_i$ is the following: A vertex environment V_i is an allowed subset of the tiling if its projection $\mathbf{P}^{\perp}V_i$ is contained in the window $\mathcal{W}$: $\mathbf{P}^{\perp}V_i \subset \mathcal{W}$. $\mathcal{C}_i$ is then identical to the set of translations $x_j^{\perp}$ which move $\mathbf{P}^{\perp}V_i$ inside $\mathcal{W}$, $\mathcal{C}_i = \{x_j^{\perp} \in \mathcal{W}, x_j^{\perp} + \mathbf{P}^{\perp}V_i \subset \mathcal{W}\}$. Such a type of set is denoted "$\mathcal{W}$-polar of $\mathbf{P}^{\perp}V_i$" by Katz and Duneau [18] in their variant of the projection method called the strip method, providing the name "polar calculus" for our approach.

To calculate the phason elastic constants we have to apply homogeneous phason strain to the TTT. Kiselev *et al.* enforced a well-defined average strain χ artificially by constructing a series of orthorhombic approximants with up to 20 000 atoms and values $|\chi_{11}|, |\chi_{22}| \leqslant 0.2$, $\chi_{12} = \chi_{21} = 0$, leaving only $\chi_6^{(1)} \equiv \chi_6$ and $\chi_8^{(1)} \equiv \chi_8$ nonzero. We apply the phason strain by continuously deforming the window $\mathcal{W}$ and its interior structure.

Two steps must be taken into account. Firstly, the corners $\boldsymbol{d}_i$ of the $\mathbb{A}_4$-Voronoi cell are shifted. In general, a phasonic strain could change which of the Voronoi corners end up as the window corners and which are projected somewhere in the interior of $\mathcal{W}$. But for $|\chi_n| < 0.03$, $n \in \{6, 8\}$ this does not happen. So the corners of the phasonically distorted window

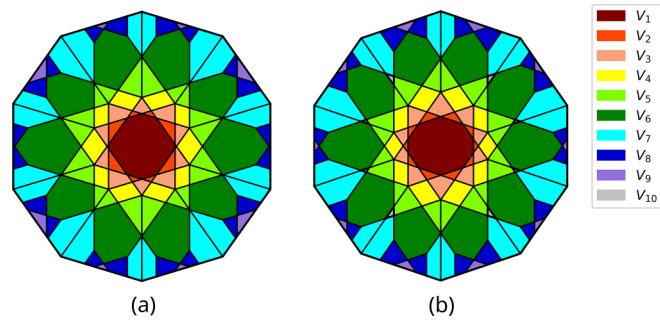

FIG. 4. Windows of phasonically distorted TTTs. (a) $\chi_6 = 0.03$, $\chi_8 = 0$. (b) $\chi_6 = 0$, $\chi_8 = 0.03$. Here, a new vertex type V_{10} appears (see Fig. 9). The windows are no longer regular decagons. The phasonic strain deforms $\mathcal{W}$, but for small χ, this change is hardly visible.

$\mathcal{W}(\chi)$ are given by

$$d_l^{\perp}(\chi) = d_l^{\perp} + \chi d_l^{\parallel}, \quad l = 1, \ldots, 10, \tag{9}$$

with the phasonic strain tensor either

$$\chi = \frac{\chi_6}{\sqrt{2}}\begin{bmatrix} 1 & 0 \\ 0 & -1 \end{bmatrix} \quad \text{or} \quad \chi = \frac{\chi_8}{\sqrt{2}}\begin{bmatrix} 1 & 0 \\ 0 & 1 \end{bmatrix}. \tag{10}$$

The hyperlattice points corresponding to the atom positions are shifted in the same manner as the Voronoi corners. So in a crystal of small but constant and homogeneous phasonic strain, Eq. (8) is generalized to

$$\mathcal{C}_i(\chi) = \bigcap_j (v_j^{\perp} + \chi v_j^{\parallel} + \mathcal{W}(\chi)). \tag{11}$$

Two examples of slightly phasonic deformed projection windows are depicted in Fig. 4. The windows remain convex, but not exactly regular decagons. There, a new vertex V_{10} appears (see Fig. 9) with energy as V_6.

We call such a homogeneously deformed tiling "flat" and denote it as $\mathcal{Q}(\chi)$. The proportion or "density" of vertices of type i in the flat tiling is $\rho_i(\chi) = |\mathcal{C}_i(\chi)|/|\mathcal{W}(\chi)|$, and its configurational potential energy per atom (or "energy density") results as

$$E(\chi) = \frac{1}{2}\sum_i \rho_i(\chi) E_i, \tag{12}$$

where the sum runs over the nine or possibly further vertices.

III. FREE ENERGY CALCULATIONS

As in quasicrystals phonon frequencies are two orders of magnitude larger than phason flip rates, one can separate their total free energy $F = F_{\mathrm{phon}} + F_{\mathrm{conf}}$ into a phonon part F_{phon}, which can be treated by molecular dynamics, and a configurational part F_{conf}, which is due to the tiling degeneracy caused by phason flips and which requires accelerated methods.

A. Phonon free energy from MD

Kiselev *et al.* calculated the phonon part in dependence of a constant average phason strain χ with a combination of the Frenkel-Ladd [24] method and thermodynamic integration as

in Ref. [25] and obtained

$$F_{\text{phon}}(\chi, T) = E_0(\chi) + T g(\chi) + I(\chi, T). \tag{13}$$

Here, $E_0(\chi)$ is the ground state energy. It is obtained from the configurational potential energy $E(\chi)$ by minimization through phason flips. The term $g(\chi)$ is an integration constant and $I(\chi, T)$ the thermodynamic integral according to Frenkel-Ladd. To obtain $E_0(\chi)$, for each approximant the energy was relaxed by Monte Carlo phason flips within the unit cell, and the binding energies of the vertex environments were summed up. They found that $g(\chi)$ and $I(\chi, T)$ are independent of χ. Hence the two terms do not contribute to the phason elastic constants and do not have to be considered further.

As already Kiselev *et al.* recognized, randomization by phason flips can lower $E(\chi)$ to the true configurational potential or "ground state" energy $E_0(\chi)$ as used in the Frenkel-Ladd method Eq. (13). To perform this relaxation and to calculate the configurational free energy with purely geometric methods, we will enlarge the polar calculus in Sec. IV.

B. Flip Ising model for the configurational free energy

Kiselev *et al.* dealt with phason flips in two ways. For energy relaxations, they used stochastic methods, namely, checking randomly whether a vertex can be flipped and performing the flip whenever it lowered the energy. To calculate the configurational free energy F_{conf}, they applied an approximation of uncorrelated flips. They restricted themselves to flips that originate in the vertices V_7, V_8, and V_9, arguing that in a small shift of the projection window, only these vertices flip as their domains are located at the boundary. There are six types $\mathcal{F}_k$, $k = 1, \ldots, 6$, of flips and they were modeled as Ising spins with flip energies $\Delta E^k = |E_2^k - E_1^k|$, $k = 1, \ldots, 6$, given as the potential energy difference of two involved vertices V_1^k and V_2^k. The configurational free energy (per atom) then results as

$$F_{\text{conf}}(\chi, T) = -k_B T \sum_k \frac{n_k(\chi)}{N(\chi)} \ln\left[1 + \exp\left(-\frac{\Delta E^k}{k_B T}\right)\right], \tag{14}$$

where $N(\chi)$ is the number of atoms in the unit cell of the approximant and $n_k(\chi)$ is the number of flips therein of type k.

C. Phason elastic constants and stability ranges

Now Kiselev *et al.* could calculate the phason elastic constants as

$$\lambda_n(T) = \frac{\partial^2 E_0(\chi)}{\partial \chi_n^2} + \frac{\partial^2 F_{\text{conf}}(\chi, T)}{\partial \chi_n^2}, \quad n \in \{6, 8\}. \tag{15}$$

$E_0(\chi)$ showed up as saddle point, ascending along the χ_6- and descending along the χ_8-direction. Thus, at $T = 0$, λ_8 resulted as negative, rendering the quasicrystal unstable. The second term for both directions was positive and increased with temperature, changing the sign of λ_8 at $T_c = 0.35 \pm 0.01$. Thus the model quasicrystal turned out to be a high-temperature phase, in accord with the random tiling hypothesis.

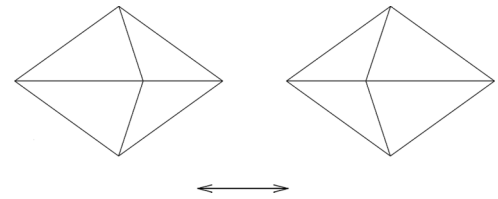

FIG. 5. Simpleton flip of the TTT.

IV. DYNAMIC POLAR CALCULUS

We are going to check the random tiling hypothesis by purely geometrical methods. From the results of Kiselev *et al.* we make use only (1) of the potential energies E_i of the vertices V_i, Eq. (5), and (2) of the fact, that the only χ-dependent part of the phonon free energy is $E_0(\chi)$. We generalize the above results by (a) enlarging the variety of flips and (b) introducing flip correlations.

A. Flip extensions and flip acceptance domains

Two types of phason strain must be distinguished. (i) The average phason strain χ, which Kiselev *et al.* realize by the deformed unit cell of the approximant and we by the homogeneously deformed projection window, and (ii) the position-dependent strain $\chi(x^{\parallel})$, which arises in flip relaxations and expresses the randomness. For the latter, we abandon the restriction of Kiselev *et al.* to flips only between vertices V_7, V_8, and V_9 and admit flips between those vertices which in the Golden Triangle subdivision allow the rhombic simpleton flip Fig. 5. Inspection shows that these are $V_4, \ldots, V_{10}$.

Let us now use the notation $\mathcal{F}(i, j)$ for a flip $V_i \to V_j$. All possible single flips that can happen in any crystal $\mathcal{Q}(\chi_n)$ with $|\chi_n| < 0.01$, $n \in \{6, 8\}$ are shown in Fig. 6. Only the ones shown in blue were considered by Kiselev *et al.*

In some clusters of Fig. 6 not only the vertices around the flipping particle but also the vertex configuration of the

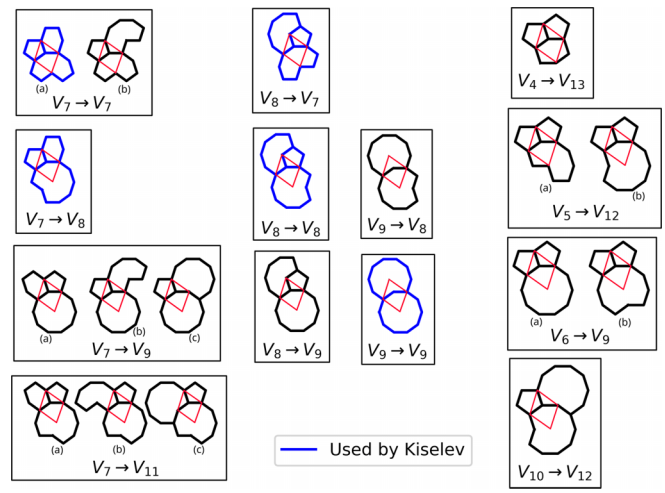

FIG. 6. All possible initial flip configurations in the crystals $\mathcal{Q}(|\chi_n| < 0.01)$, $n \in \{6, 8\}$, together with the vertices within the interaction radii of initial and final flip position. For some flips $\mathcal{F}(i, j)$, there are several tile combinations labeled (a), (b), etc.

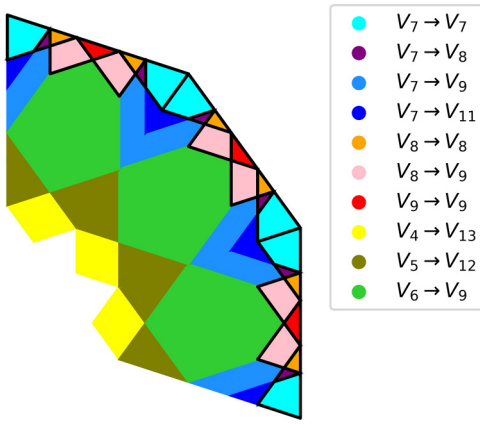

FIG. 7. Flip windows in the ideal TTT. The areas outlined in black correspond to flips that were used by Kiselev *et al.*

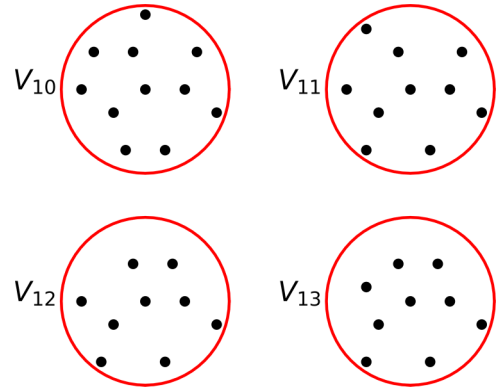

FIG. 9. New vertices that appear due to phasonic strain, or due to single flips. The red circle marks the interaction radius of the central atom.

flipping particle itself will not be one of $V_1, \ldots, V_{10}$ after the flip. The new vertex types that emerge this way are called V_{11}, V_{12}, and V_{13}, see Fig. 9. Their potential energies are $E_{11} = -9.3$, $E_{12} = -7.9$, and $E_{13} = -6.7$. The energies of V_{12} and V_{13} are very high compared to the vertices $V_1, \ldots, V_{11}$, making flips that result in states V_{12}, V_{13} very unlikely for temperatures T below the melting temperature T_m.

Now we can use the vertex configurations of Fig. 6 to construct *flip domains* $\mathcal{P}_k$ in exactly the same way as the domains $\mathcal{C}_i$ of the vertices V_i, Eqs. (8) and (11). They allow to calculate densities $\nu_k \equiv n_k/N$ of flip type k as for example used in Eq. (14), as $\nu_k = |\mathcal{P}_k(\chi)|/|\mathcal{W}(\chi)|$. In each arrangement, the flip atom was chosen as the reference atom and placed at the origin. The domains are shown in Fig. 7 for $\chi = 0$ and in Fig. 8 for $\chi = 0.03$ with three orientations. For the perfect tiling ($\chi = 0$), one orientation would be already sufficient. For $\mathcal{Q}(\chi \neq 0)$, three segments are required and suffice because the phasonic strain matrices in $\chi_6^{(1)}$ and $\chi_8^{(1)}$-directions commute with the reflections in x and y directions, from which all other orientations of the flip domains result. The flips in the outlined black areas were used by Kiselev.

B. Analytical ground state relaxation

We are ready to approximately relax the energy $E(\chi)$ of Eq. (12) of the flat tiling to $E_0(\chi)$ of a random tiling with our geometric tool. In the flat tilings, we look for atom configurations whose energy can be lowered by a single flip. Of these, there are only two types, the flips $\mathcal{F}(8,7)$ and $\mathcal{F}(9,8)$. All other flips are already in their low-energy state. So, for the relaxation, we assign to every atom with a local configuration $\mathcal{F}(8,7)$ the energy E_7 and to every atom with configuration $\mathcal{F}(9,8)$ the energy E_8. In other words, we subtract the energy per particle $\nu_{\mathcal{F}(8,7)}E_8$ and replace it by the flipped energy $\nu_{\mathcal{F}(8,7)}E_7$, and the same for $\mathcal{F}(9,8)$:

$$E_0(\chi) = \frac{1}{2}\sum_i \rho_i(\chi)E_i + \nu_{\mathcal{F}(8,7)}(E_7 - E_8) + \nu_{\mathcal{F}(9,8)}(E_8 - E_9). \tag{16}$$

Interestingly such energy-lowering single flips only show up for $\chi \neq 0$.

Surely, the energy could be still lowered by including the effects of correlated flips. However, as we will see below, it already contains the seed for a low-temperature instability of the quasicrystal and is not changed by nearest neighbor correlations as dealt with in the following pentagon coupling model.

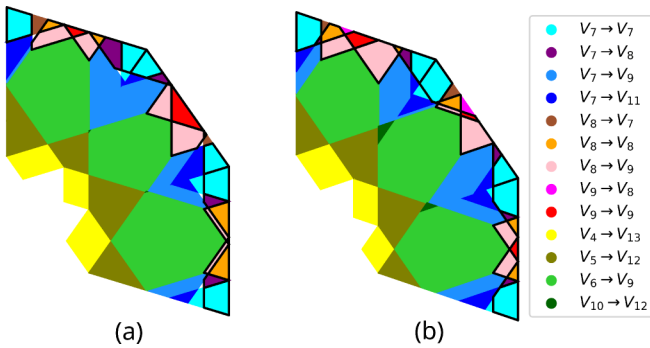

FIG. 8. Flip windows in the phasonically distorted TTT $\mathcal{Q}(\chi)$. (a) $\chi_6 = 0.03$ and (b) $\chi_8 = 0.03$.

C. Flip correlations and pentagon coupling

The flip Ising model of Sec. III B ignores the fact, that two neighboring particles cannot flip simultaneously. In the examples of Fig. 10, the blue and red particles are strongly correlated because each is a corner point of the other particle's flip rhombus. The corners of the overlapping rhombi form a pentagon. By flipping consecutively the particles create ten states, which are $2\pi/10$ rotated about the bottom anchor

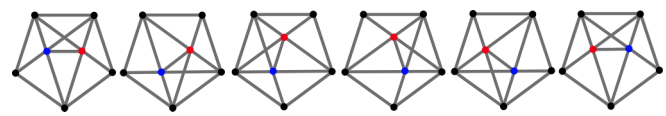

FIG. 10. Two nearest neighbor flips are correlated in such a way that one particle is a corner point on the side of the other particle's rhombus. Six consecutive flip states are shown. Each state is related to all other states by some D_{10}-operation. The flip particles can never leave the pentagon that is defined by their rhombi.

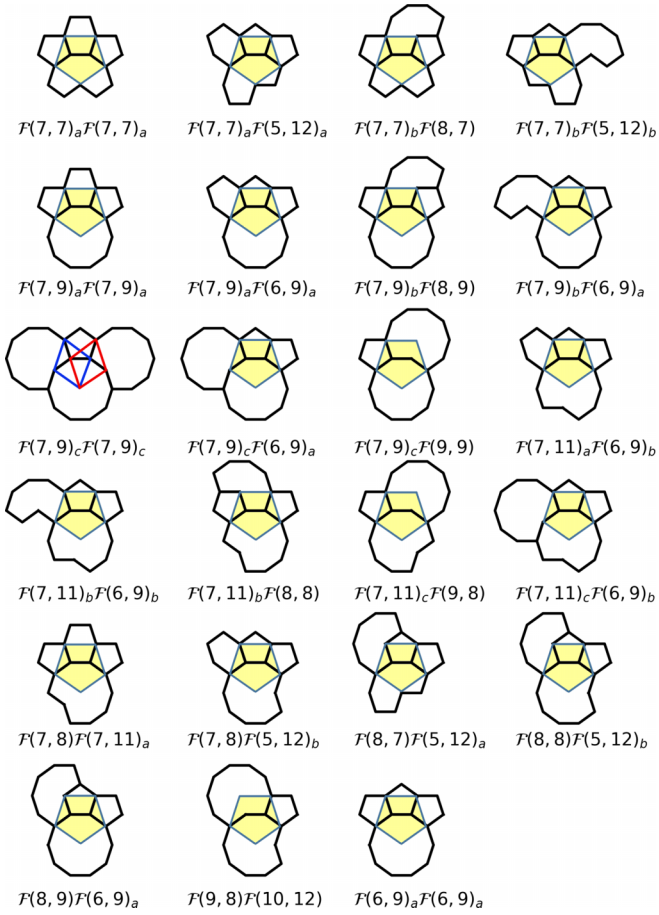

FIG. 11. All PC clusters in flat crystals $\mathcal{Q}(|\chi| < 0.01)$, marked by yellow pentagons, and their surroundings. The two correlated flips are oriented as shown by the small rhombi in one of the figures.

point. After five flips, the initial sequence repeats but with blue and red exchanged, so there are pairs of degenerate states. The pentagon represents a generic version of coupled particles, which may be embedded in an arbitrary, but fixed environment. This kind of nearest neighbor coupling is almost ubiquitous in the crystals $\mathcal{Q}(\chi)$, see also Fig. 2. Except for $\mathcal{F}(4, 13)$, the flipping vertex of all flip types in Fig. 6 is part of such a pair of $2\pi/10$-rotated rhombi. Due to this local symmetry, we will call this type of correlation *pentagon coupling* (PC).

We want to identify all neighborhoods of the pentagons of that minimal size, which suffices to determine precisely the energies of the five states. All required neighbor atoms must be within the interaction radii of both flipping particles for all their positions. These environments will be called *PC clusters*. Since the flips shown in Fig. 6 are all possible single flips in any crystal $\mathcal{Q}(|\chi| < 0.01)$, each PC cluster must contain some combination of them. Further surrounding atoms could be necessary. Luckily, it turns out that all PC clusters are found simply by adding one extra tile to the single flip configurations. In total, 23 types of PC clusters are found in the crystals $\mathcal{Q}(|\chi| < 0.01)$. They are shown in Fig. 11. A PC cluster is labeled $\mathcal{F}(i, j)\mathcal{F}(k, l)$, where $\mathcal{F}(i, j)$ is the flip on the left side and $\mathcal{F}(k, l)$ is the flip on the right side, provided that the cluster is oriented such that the common anchor point of the two rhombi is pointing downwards as in the picture. Note that

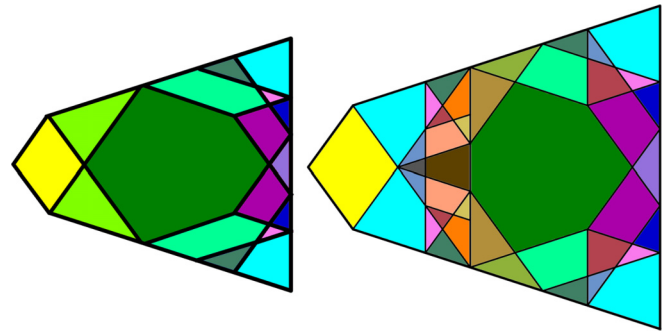

FIG. 12. A section of the window for $\chi = 0$ with the domains for the flips as in Fig. 6 and the further subdivision for the PC clusters as in Fig. 11.

the cluster $\mathcal{F}(k, l)\mathcal{F}(i, j)$ is just a reflection of $\mathcal{F}(i, j)\mathcal{F}(k, l)$ and is not shown.

In the same way, as we found the domains of the single flip configurations, we can also compute the domains of the PC clusters. They were calculated with respect to one of the flip atoms as a reference so that they lay within the same flip window as the single flips. The PC domains subdivide and decompose the single flip domains as shown in Fig. 12. The new domains should just cover the single flip domains completely, except for the one of $\mathcal{F}(4, 13)$, to prove that all PC clusters were found.

D. Extended free energy model

The pentagonal coupled clusters consider not only the single flips as in the flip Ising model but also the correlations between the flips of two neighboring particles, which results in a total of ten states with at most five different energies. But each PC cluster is just as independent of the rest of the crystal as the single flips were in the flip Ising model, introduced in Sec. III B. Hence the PC clusters can also be treated as independent "spins," but with ten states instead of two, also denoted Potts model [19]. Each PC cluster will be of some type $k \in \{1, \ldots, 23\}$, and each type of cluster has some density $\nu_k^{\mathrm{pc}}(\chi)$, that we obtain from the polar calculus. Furthermore, each state of a PC cluster has an energy E_i^k. It is simply the sum of the potential energies of the two flip atoms,

$$E_i^k = \sum_l V_{\mathrm{LJG}}\big(|r_l^k - q_i|\big) + \sum_l V_{\mathrm{LJG}}\big(|r_l^k - q_i + \Delta q_i|\big) + V_{LJG}(|\Delta q_i|), \tag{17}$$

where r_l^k are the positions of the surrounding atoms of the type-k PC cluster, q_i is the position of the blue particle in state i and Δq_i are vectors from the blue to the red atoms in Fig. 10. Because the PC clusters are complete with respect to the cutoff radius $r_c = 2$, the energy differences $|E_i^k - E_j^k|$ of two adjacent states are equivalent to the flip energies ΔE^k as defined in the single flip-Ising model. We normalize the energies of the PC-states such that the total configurational free energy of PC clusters vanishes at $T = 0$. So, if E_{g}^k is the lowest possible energy of a type-k PC cluster, the states with energies E_i^k get assigned the effective energy $\Delta E_i^k = E_i^k - E_{\mathrm{g}}^k \geqslant 0$. The normalized canonical partition sum of one type-k PC cluster

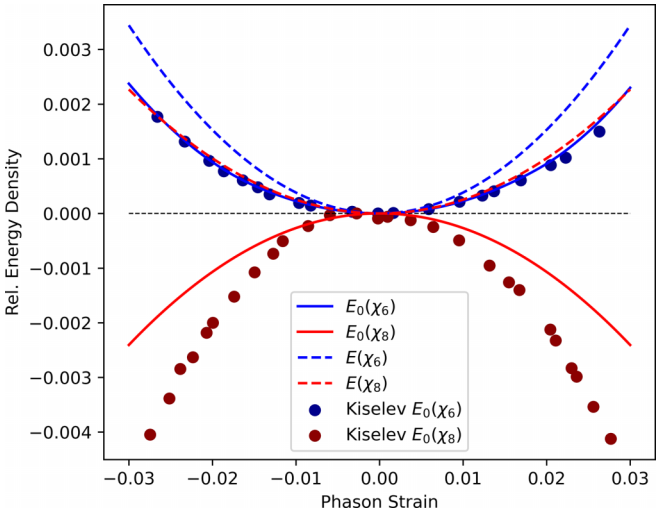

FIG. 13. Offset adjusted ground state energies: blue along χ_6, red along χ_8 direction. Dashed lines come from the homogeneously phason deformed windows [Eq. (12)], full lines after geometric relaxation [Eq. (16)]. The single dots stem from MD simulations by Kiselev [26].

reads

$$Z_k^{\rm pc} = \sum_{i=1}^{10} e^{-\Delta E_i^k/k_BT} = 2\sum_{i=1}^{5} e^{-\Delta E_i^k/k_BT}. \tag{18}$$

The labels i are supposed to be ordered like the consecutive flip states in Fig. 10 so that we can use $E_i^k = E_{(i+5)\text{mod}10}^k$. Then the configurational free energy density of PC clusters in the whole crystal, $F_c^{\rm pc}$ follows as

$$F_{\rm config}^{\rm pc}(T,\chi) = -k_BT\sum_{k=1}^{23} \nu_k^{\rm pc} \ln Z_k^{\rm pc}. \tag{19}$$

V. RESULTS

A. Ground state energy

The energy per atom of the perfect ("flat") TTT according to Eq. (6), determined with the polar calculus of the window in Fig. 2 and the data of Table I, yields the value $E(\chi = 0) = -6.647$. As for $\chi = 0$, there are no energy lowering flips in the geometric relaxation according to Eq. (16), the ground state energy $E_0(\chi = 0)$ has the same value, in excellent agreement with the MC result of Kiselev $E_0^K(\chi = 0) = -6.649$.

The full χ-dependent energies are shown in Fig. 13. They carry an approximate parabolic shape. For comparison of the curvatures, they are shifted vertically to meet at the origin. Dashed curves come from Eq. (12), where the densities were found from the homogeneously phason deformed window as in Fig. 4, right. Upon geometric relaxation by flips $\mathcal{F}(8,7)$ and $\mathcal{F}(9,8)$ as in Eq. (16) we obtain the full curves. For χ_6 (blue) the curvature decreases but remains positive. However, the parabola for χ_8 (red) turns downward. The relaxed energy over the $\chi_6 - \chi_8$ plane presents a saddle point. This is the essence of the present studies, since as a consequence of Eq. (15) the phason elastic constant λ_8 is negative at $T = 0$ and the quasicrystal unstable. Indeed, according to

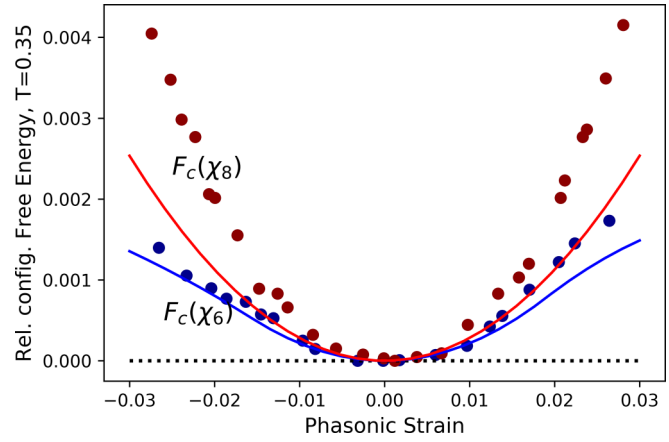

FIG. 14. Offset adjusted configurational free energy in the flip Ising model $F_{\rm config}(\chi_n, T)$ for $n = 6$ in blue, $n = 8$ in red and $T = 0.35$. Both analytical curves are calculated using the flip densities for a flat crystal $\mathcal{Q}(\chi)$. Dots were measured by Kiselev [26] in MC simulations for the relaxed state.

Engel *et al.* at $T = 0$ a transformation to the approximant Xi phase occurs during annealing simulations with the LJG-potential. The dotted points are the MC results of Kiselev *et al.* They agree remarkably well with the geometric results for χ_6 but have a larger negative curvature for χ_8. The reason might be that in MC higher-order correlations were effective [while the two-particle correlations of the pentagon coupling model are fully taken regard of in our geometric relaxation Eq. (16)].

The curvatures $\partial^2_{\chi_6} E_0(\chi_6)$, $\partial^2_{\chi_8} E_0(\chi_8)$ express the values of the phasonic constants at $T = 0$ and are listed below. We add the curvatures of $E_0^{(\rm K)}(\chi)$ obtained by Kiselev, denoted $\lambda^{(\rm K)}(0)$, which were extracted from his master thesis [26].

$$\lambda_6(0) = 2.265, \quad \lambda_8(0) = -2.676,$$
$$\lambda_6^{(\rm K)}(0) = 2.314, \quad \lambda_8^{(\rm K)}(0) = -5.318. \tag{20}$$

B. Configurational free energy in the flip-Ising model

The dynamic polar calculus of Sec. IV leads to the flip domains in Figs. 7 and 8 and allows to extract the flip densities $\nu_k(\chi) = n_k(\chi)/N(\chi) = |\mathcal{P}_k(\chi)|/|\mathcal{W}(\chi)|$ geometrically, whereas they were counted numerically by Kiselev *et al.* Taking the flip types used by Kiselev *et al.* (in the figures outlined in black) and the vertex energies from Table I we obtain the configurational free energy for the flip Ising model according to Eq. (14). For $T = 0.35$ this free energy is plotted in Fig. 14, height adjusted as only the curvatures are of relevance. Close to $\chi = 0$ it shows up as parabolic. The positive curvature of $F_{\rm config}(\chi_8, T = 0.35)$ slightly overcompensates the negative one of $E_0(\chi_8)$, so that $\lambda_8(T = 0.35)$ just has overcome the phason softening point, see Fig. 15. In general, the curvature of the configurational free energy is monotonically increasing with temperature.

The agreement for $\lambda_6(T)$ is very good. The values for $\lambda_8(T)$ start lower as already seen in Eq. (20). Remarkably, very similar stabilization temperatures (0.33 and 0.35) are predicted by both models. The random tiling hypothesis is

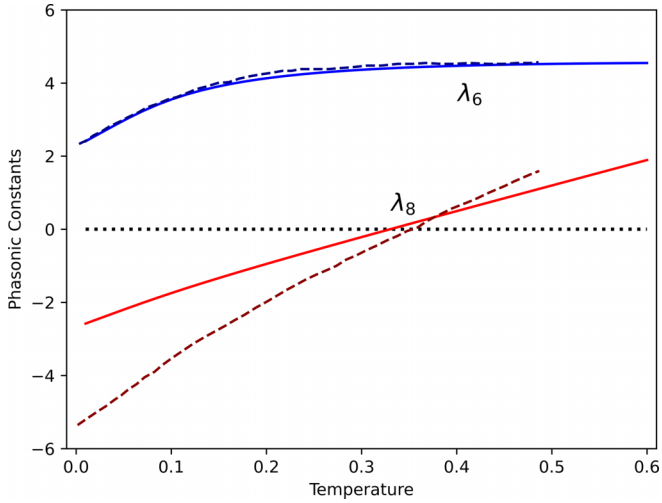

FIG. 15. Phason elastic constants over temperature. Dashed lines are numeric results $\lambda_n^{(K)}(T)$ from Ref. [9]. The continuous curves $\lambda_n(T)$ were calculated using the approximation of independent single flips for E_0 and F_c. The melting temperature in MD simulations is $T = 0.56$.

confirmed, as $F \propto |\chi|^2$ and as the quasicrystal becomes stable only at elevated temperatures.

C. Configurational free energy with correlations

Now, in the configurational free energy, we take regard of all flips as pictured in Figs. 7 and 8 apart from flip $\mathcal{F}(4, 13)$, which has by far the highest flip energy $\Delta E_k = 9.321$ and does not contribute to F_{config}. We furthermore take into account nearest neighbor correlations of flips as realized in the 23 PC clusters of Fig. 11 and in the ten-state Potts model, and calculate the configurational free energy according to Eq. (19). It is presented in Fig. 16 for $T = 0.35$ and close to $\chi = 0$ has a parabolic form.

We use two offset values for the zero temperature elastic constants as in Eq. (20). The first is based on the ground state

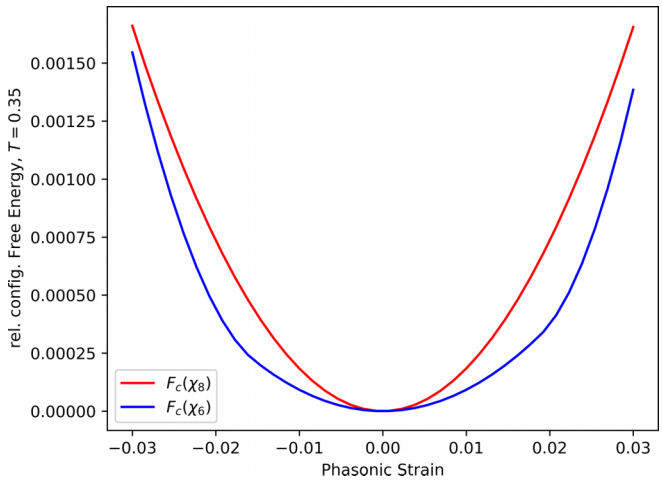

FIG. 16. Offset adjusted configurational free energy in the ten-state Potts model $F_{\text{config}}(\chi_n, T)$ for $n = 6$ in blue, $n = 8$ in red, and $T = 0.35$.

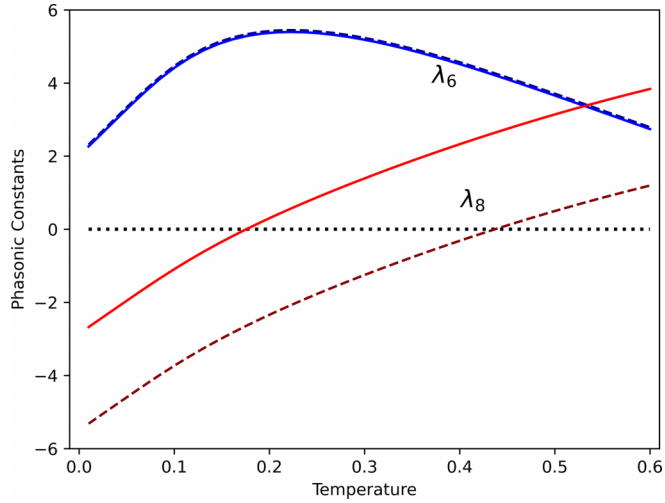

FIG. 17. Phasonic constants from the model of PC clusters. The dashed lines are those with the offset at $T = 0$ from MC simulations as given in Eq. (20).

energy $E_0(\chi)$, Eq. (16), which was obtained from relaxing the flat energy Eq. (12) by uncorrelated flips $\mathcal{F}(8, 7)$ and $\mathcal{F}(9, 8)$. The second, $\lambda_8^{\text{K}}(T = 0)$, comes from the numerical simulations of Kiselev.

The temperature dependence of the phason elastic constants is displayed in Fig. 17. The model with the geometrically relaxed ground state energy shows a low soft phason transition at $T = 0.22$. With the numerical values, we obtain $T = 0.45$. With both offsets, the results prove a low-temperature instability of the quasicrystal and confirm the random tiling hypothesis.

VI. DISCUSSION AND SUMMARY

Quasicrystals are not periodic and possess a confusingly large number of local environments. Fortunately, there is an efficient bookkeeping method for the environments, denoted polar calculus [18]. The discrete vertices of the infinite quasicrystal can be mapped one-to-one onto a polygon of finite size, which is denoted window $\mathcal{W}$ and necessarily is filled densely. In the case of the Tübingen triangle tiling (TTT)—the object of our present studies—the window is a regular decagon. Any local environment repeats infinitely often, can be associated with a subdomain $\mathcal{C}_i$ of the window and thus given its relative portion in the structure. The polar calculus is the exclusive geometric tool in our endeavor to confirm the random tiling hypothesis. In a previous study by Kiselev *et al.* [9] a random version of the TTT could be grown in molecular dynamics simulations with a Lennard-Jones-Gauß double well potential V_{LJG}. In the ideal TTT, nine types of vertex environments V_i exist within an effective interaction radius of $r_{\text{int}} = 2$. Their relative occurrence ρ_i can be determined by the area $|\mathcal{C}_i|$ of their domain $\mathcal{C}_i$, and their potential energy E_i by application of the potential V_{LJG}. Uniform phason strain χ is applied to the ideal TTT by homogeneous phason deformation of the window and its interior subdivision, leading to four more vertex environments. The procedure allows us to

calculate a "flat" energy density $E(\chi) = \sum_i \rho_i(\chi) E_i$. As shown by Kiselev *et al.* with a method of Frenkel-Ladd and thermodynamic integration [24,25] a flip relaxed version $E_0(\chi)$ of this energy density is the only χ-dependent part of the phonon contribution to the free energy density $F(\chi, T)$ and is its value at $T = 0$. The second derivatives of $F(\chi, T)$ with respect to χ yield the phason elastic constants. We analyzed the minimal interaction environments for all simpleton flips, a total of 13, and constructed corresponding flip domains $\mathcal{P}_k(\chi)$ in the window $\mathcal{W}(\chi)$. Whenever a flip lowered the energy, we replaced the initial vertex by the flipped one in the flat energy density and thus approximated $E_0(\chi)$. In this way, we arrived at a random tiling. It turned out that $E_0(\chi = 0)$ shows a saddle point, rendering one of the phason elastic constants, $\lambda_8(T = 0)$, negative and hence the quasicrystal unstable at $T = 0$. Kiselev *et al.* [9] had arrived at the ground state energy $E_0(\chi)$ by performing Monte Carlo flips in approximants. Their value of $\lambda_8^{(\mathrm{K})}(0)$ also turned out negative, but twice as deep as with our geometric method.

The phonon part must be supplemented by the configurational part of the free energy density $F_{\mathrm{config}}(\chi, T)$, caused by the phason degree of freedom in the form of vertex flips. Kiselev *et al.* modeled F_{config} by associating with each flip an Ising spin, however only for flips between vertices at the boundary of the decagonal window. Knowing their density from the restricted flip domains, we could reproduce the results of Kiselev *et al.* in acceptable approximation: The phason elastic constant $\lambda_6(T)$ remained positive over the entire temperature interval. The constant $\lambda_8(T)$ turned positive and stabilized the quasicrystal at $T = 0.33$, compared with previously $T = 0.35$.

Yet the flip Ising model neglects correlations between flipping spins. If two rhombi overlap, forming a pentagon as in Fig. 10, the flipping vertex of one is the corner point of the other. A simpleton flip of the first changes the flip direction and energies of the second. Flipping the second vertex and continuing one creates ten states in the pentagon. It turns out that 12 of the 13 interaction environments for simpleton flips contain the overlapping rhombi. We identified 23 neighborhoods where the atoms are within the interaction radius of the overlapping rhombi and all the flipped states of the pentagon and denoted them pentagon coupled (PC) clusters. These not only encompass the single spin flips but also their correlations. The PC clusters represent ten-state Potts models and replace the two-state Ising spin model. To calculate the configurational free energy F_{config}, we determine the energy E_i^k of each Potts state i in the PC cluster k with the interaction potential V_{LJG}. Furthermore, the density ν_k^{pc} is required and found with the help of the domains $\mathcal{P}_k(\chi)$ of the PC clusters in the window $\mathcal{W}(\chi)$. Also in this refined model, the random tiling hypothesis is confirmed: the free energy is proportional to $|\chi|^2$ and the quasicrystal is unstable at low temperatures due to a negative phason elastic constant λ_8.

However, as evident from Fig. 17, the stabilization temperature goes down from $T = 0.35$ to $T = 0.17$. The reason is the high offset value $\lambda_8(0) = -2.676$ from Eq. (20). With the value $\lambda_8^{(\mathrm{K})}(0) = -5.318$ of Kiselev *et al.* [9,26] it is shifted up to $T = 0.42$. What is the reason for the difference? Our geometric relaxation of the energy density $E(\chi)$ to the ground state energy $E_0(\chi)$ was performed by two types of energy-reducing single flips, namely vertices V_8 to V_7 and V_9 to V_8. No correlations were taken regard of, in contrast to the unlimited number of correlations in the relaxation by Monte Carlo flips of Kiselev *et al.* While our geometric method deals only with a localized randomization, the MC simulations of the ground state energy also contain phason flips propagating longer distances. For zero phason strain, there are no energy-lowering flips and the ground state energy for both methods excellently agrees. For $\chi_8 \neq 0$, the MC relaxation of the approximants strongly reduces the ground state energy as seen in Fig. 13. An open question is why the geometric and numeric methods only disagree for the ground state energy along χ_8 and not along χ_6.

Thus we conclude, that for the offset the numerical calculations according to Kiselev *et al.* [9,26] are to be trusted more, for the temperature dependence the pentagon cluster model, the combination of both being represented by the dashed lines in Fig. 17.

While the ground state energy $E_0(\chi)$ is easily accessible to numerical methods, the real problem is the free energy $F_{\mathrm{config}}(\chi, T)$. First, it was modeled by an ensemble of Ising spins. To calculate the density of spins, the polar calculus had to be extended to a dynamic one, where the window is divided into domains for the different spin types. Then, the model was refined further to a Potts model, which took regard of two-site correlations of the flips and also required the polar calculus. The refinement with the correlations influenced the temperature dependence of the phason elastic constants but left the conclusion untouched that quasicrystals are entropy-stabilized and high-temperature phases.

APPENDIX: COORDINATES

Symmetry adapted orthonormal bases $\{\boldsymbol{b}_x^{\parallel}, \boldsymbol{b}_y^{\parallel}\}$ of $E^{\parallel}$ and $\{\boldsymbol{b}_x^{\perp}, \boldsymbol{b}_y^{\perp}\}$ of $E^{\perp}$ are given with respect to the canonical basis $\{\boldsymbol{e}_i, i, \ldots, 5\}$ of $\mathbb{R}^5$

$$\boldsymbol{b}_x^{\parallel} = \sqrt{\frac{1}{2\sqrt{5}\tau}} \begin{bmatrix} 1 \\ -1 \\ -\tau \\ 0 \\ \tau \end{bmatrix}, \quad \boldsymbol{b}_y^{\parallel} = \sqrt{\frac{1}{10}} \begin{bmatrix} \tau \\ \tau \\ -1/\tau \\ -2 \\ -1/\tau \end{bmatrix},$$
$$\boldsymbol{b}_x^{\perp} = \sqrt{\frac{1}{2\sqrt{5}\tau}} \begin{bmatrix} \tau \\ -\tau \\ 1 \\ 0 \\ -1 \end{bmatrix}, \quad \boldsymbol{b}_y^{\perp} = \sqrt{\frac{1}{10}} \begin{bmatrix} 1/\tau \\ 1/\tau \\ -\tau \\ 2 \\ -\tau \end{bmatrix}. \tag{A1}$$

These vectors, together with the canonical bases $\{e_x^{\parallel}, e_y^{\parallel}\}$ on $E^{\parallel}$ and $\{e_x^{\perp}, e_y^{\perp}\}$ on $E^{\perp}$, define the projection operators

$$\mathbf{P}^{\parallel} = e_x^{\parallel} \boldsymbol{b}_x^{\parallel t} + e_y^{\parallel} \boldsymbol{b}_y^{\parallel t}, \quad \mathbf{P}^{\perp} = e_x^{\perp} \boldsymbol{b}_x^{\perp t} + e_y^{\perp} \boldsymbol{b}_y^{\perp t}. \tag{A2}$$

The window $\mathcal{W}$ in the TTT is defined as the $\mathbf{P}^{\perp}$ projection of the $\mathbb{A}_4$ lattices' Voronoi cell $\mathcal{V}_{\mathbb{A}_4} = \mathcal{V}_{\mathbb{A}_4}(\mathbf{0})$ around

TABLE II. Three of the corners of the windows, represented in different spaces. The other corners are found by all possible x and y reflections of these.

$\boldsymbol{d} \in \mathcal{H}$	$d^\perp \in E^\perp$	$d^\parallel \in E^\parallel$
$\frac{1}{2}(\widetilde{\boldsymbol{a}}_0+\widetilde{\boldsymbol{a}}_1-\widetilde{\boldsymbol{a}}_2+\widetilde{\boldsymbol{a}}_3-\widetilde{\boldsymbol{a}}_4)$	$\left(0, \sqrt{\frac{2}{5}}\tau\right)$	$\left(0, \sqrt{\frac{2}{5}}\frac{1}{\tau}\right)$
$\frac{1}{2}(-\widetilde{\boldsymbol{a}}_0+\widetilde{\boldsymbol{a}}_1-\widetilde{\boldsymbol{a}}_2+\widetilde{\boldsymbol{a}}_3-\widetilde{\boldsymbol{a}}_4)$	$\left(-\sqrt{\frac{\tau}{2\sqrt{5}}}, \frac{\tau^2}{\sqrt{10}}\right)$	$\left(-\sqrt{\frac{1}{2\sqrt{5}\tau}}, -\frac{1}{\sqrt{10}}\frac{1}{\tau^2}\right)$
$\frac{1}{2}(-\widetilde{\boldsymbol{a}}_0+\widetilde{\boldsymbol{a}}_1-\widetilde{\boldsymbol{a}}_2+\widetilde{\boldsymbol{a}}_3+\widetilde{\boldsymbol{a}}_4)$	$\left(-\sqrt{\frac{\tau^3}{2\sqrt{5}}}, \frac{1}{\sqrt{10}}\right)$	$\left(\sqrt{\frac{1}{2\sqrt{5}\tau^3}}, -\frac{1}{\sqrt{10}}\right)$

the origin

$$\mathcal{V}_{\mathbb{A}_4} = \{\boldsymbol{x} \in \mathcal{H}, \quad |\boldsymbol{x}| < |\boldsymbol{v} - \boldsymbol{x}| \ \ \forall\, \boldsymbol{0} \neq \boldsymbol{v} \in \mathbb{A}_4\}. \tag{A3}$$

To construct $\mathcal{V}_{\mathbb{A}_4}$ more concrete the dual lattice $\widetilde{\mathbb{A}_4}$ of $\mathbb{A}_4$ will be useful. Up to a factor of 2π, this is the same as the reciprocal lattice

$$\widetilde{\mathbb{A}_4} = \{\boldsymbol{x} \in \mathcal{H}, \quad \boldsymbol{x} \cdot \boldsymbol{v} \in \mathbb{Z} \ \ \forall\, \boldsymbol{v} \in \mathbb{A}_4\}. \tag{A4}$$

A basis of $\widetilde{\mathbb{A}}_4$ is given by

$$\left\{\widetilde{\boldsymbol{a}}_i = \boldsymbol{e}_i - \frac{1}{5}\Delta, \ i = 0, 1, 2, 3, 4\right\}, \qquad \text{where } \Delta = \sum_{i=1}^{5} \boldsymbol{e}_i. \tag{A5}$$

It can be shown that $|\sum_i \lambda_i \widetilde{\boldsymbol{a}}_i| < |\boldsymbol{v} - \sum_i \lambda_i \widetilde{\boldsymbol{a}}_i|$ for all $\boldsymbol{v} \in \mathbb{A}_4$ and $|\lambda_i| < 1/2$. So the Voronoi cell of $\mathbb{A}_4$ can be written as

$$\mathcal{V}_{\mathbb{A}_4} = \left\{ \sum_i \lambda_i \widetilde{\boldsymbol{a}}_i, \ \ |\lambda_i| < \frac{1}{2} \right\}. \tag{A6}$$

Projecting $\mathcal{V}_{\mathbb{A}_4}$ onto $E^\perp$ yields a decagon as shown in the right of Fig. 1. For the correct construction of the TTT, it must be half open, similar as for the Fibonacci chain. Otherwise, there would be "forbidden" distances between some atoms, corresponding to overlapping tiles. This half-open condition has no consequences for the polar calculus though, as it does not change the window's area. $\mathcal{W}$ is parameterized by its corners $d_i^\perp$, $i = 1, \ldots, 10$. These corners are $E^\perp$ projections of some of the corners $\boldsymbol{d}_i$ of the root lattice's Voronoi cell. They are best expressed in the basis $\{\widetilde{\boldsymbol{a}}_i, \ \ i = 0, 1, 2, 3, 4\}$ of the dual space $\widetilde{\mathbb{A}}_4$ and written explicitly in Table II together with their $E^\perp$ and $E^\parallel$ projections.

[1] W. Steurer and S. Deloudi, *Crystallography of Quasicrystals*, 1st ed., Springer Series in Material Science Vol. 126 (Springer-Verlag, Berlin, Heidelberg, 2009).

[2] M. Baake and U. Grimm, *A Mathematical Invitation*, 3rd ed., Aperiodic Order Vol. 2 (Cambridge University Press, Cambridge, 2013), p. 263.

[3] J. E. S. Socolar, T. C. Lubensky, and P. J. Steinhardt, Phonons, phasons, and dislocations in quasicrystals, Phys. Rev. B **34**, 3345 (1986).

[4] V. Elser, Comment on "Quasicrystals: A new class of ordered structures", Phys. Rev. Lett. **54**, 1730 (1985).

[5] C. L. Henley, Random tilings with quasicrystal order: transfer-matrix approach, J. Phys. A: Math. Gen. **21**, 1649 (1988).

[6] C. Henley, Random tiling models, in *Quasicrystals: The State of the Art*, edited by D. DiVincenzo and P. Steinhardt (World Scientific Publishing, Singapore, 1991), p. 429.

[7] D. Shechtman, I. Blech, D. Gratias, and J. W. Cahn, Metallic phase with long-range orientational order and no translational symmetry, Phys. Rev. Lett. **53**, 1951 (1984).

[8] D. Gratias and M. Quiquandon, Discovery of quasicrystals: The early days, C. R. Phys. **20**, 803 (2019).

[9] A. Kiselev, M. Engel, and H.-R. Trebin, Confirmation of the random tiling hypothesis for a decagonal quasicrystal, Phys. Rev. Lett. **109**, 225502 (2012).

[10] M. Baake, P. Kramer, M. Schlottmann, and D. Zeidler, Planar patterns with fivefold symmetry as sections of periodic structures in 4-space, Int. J. Mod. Phys. B **04**, 2217 (1990).

[11] M. Engel and H.-R. Trebin, Self-assembly of monatomic complex crystals and quasicrystals with a double-well interaction potential, Phys. Rev. Lett. **98**, 225505 (2007).

[12] M. Engel and H.-R. Trebin, Stability of the decagonal quasicrystal in the Lennard-Jones-Gauss system, Philos. Mag. **88**, 1959 (2008).

[13] P. Bancel, Dynamical phasons in a perfect quasicrystal, Phys. Rev. Lett. **63**, 2741 (1989).

[14] Y. Ishii, Phason softening and structural transitions in icosahedral quasicrystals, Phys. Rev. B **45**, 5228 (1992).

[15] H.-R. Trebin, U. Koschella, M. Umezaki, and T. Odagaki, Investigation of phason statics and dynamics, Philos. Mag. **86**, 1021 (2006).

[16] X. Zeng, G. Ungar, Y. Liu, V. Percec, A. E. Dulcey, and J. K. Hobbs, Supramolecular dendritic quasicrystals, Nature (London) **428**, 157 (2004).

[17] K. Hayashida, T. Dotera, A. Takano, and Y. Matsushita, Polymeric quasicrystal: Mesoscopic quasicrystalline tiling in *ABC* star polymers, Phys. Rev. Lett. **98**, 195502 (2007).

[18] A. Katz and M. Duneau, Quasiperiodic patterns and icosahedral symmetry, J. Physique **47**, 181 (1986).

[19] F. Y. Wu, The Potts model, Rev. Mod. Phys. **54**, 235 (1982).

[20] E. Fayen, L. Filion, G. Foffi, and F. Smallenburg, Quasicrystals of binary hard spheres on a plane stabilized by configurational entropy, Phys. Rev. Lett. **132**, 048202 (2024).

[21] W. Ludwig and C. Falter, *Symmetry in Physics: Group Theory Applied to Physical Problems*, 2nd ed., Springer Series in Solid State Sciences Vol. 64 (Springer-Verlag, Berlin, Heidelberg, 1996), p. 999.

[22] U. Koschella, F. Gähler, J. Roth, and H.-R. Trebin, Phason elastic constants of a binary tiling quasicrystal, J. Alloys Compd. **342**, 287 (2002).

[23] https://pypi.org/project/shapely/

[24] D. Frenkel and A. J. C. Ladd, New Monte Carlo method to compute the free energy of arbitrary solids. Application to the

fcc and hcp phases of hard spheres, J. Chem. Phys. **81**, 3188 (1984).

[25] M. Engel, Entropic stabilization of tunable planar modulated superstructures, Phys. Rev. Lett. **106**, 095504 (2011).

[26] A. Kiselev, Phasonen in quasikristallinen Strukturen des Lennard-Jones-Gauß-Systems, Master thesis, University of Stuttgart, 2011, https://stg.ibs-bw.de/aDISWeb/app?service=direct/0/Home/$DirectLink&sp=SOPAC02.